Adaptive Transient Solution of Nonuniform Multiconductor Transmission Lines Using Wavelets

S. Grivet-Talocia

***Abstract*—This paper presents a highly adaptive algorithm for the transient simulation of nonuniform interconnects loaded with arbitrary nonlinear and dynamic terminations. The discretization of the governing equations is obtained through a weak formulation using biorthogonal wavelet bases as trial and test functions. It is shown how the multiresolution properties of wavelets lead to very sparse approximations of the voltages and currents in typical transient analyzes. A simple yet effective time–space adaptive algorithm capable of selecting the minimal number of unknowns at each time iteration is described. Numerical results show the high degree of adaptivity of the proposed scheme.**

***Index Terms*—Electromagnetic (EM) transient analysis, multiconductor transmission lines (TLs), wavelet transforms.**

I. Introduction

ONE of the problems that Prof. Wait considered in his vast scientific production is propagation of electromagnetic (EM) fields in stratified media [28]. It is well known [27] that, at least in the one-dimensional (1-D) case, this problem is fully equivalent to propagation along nonuniform transmission lines (TLs), where the characteristic impedance and propagation constant can be either piecewise constant or continuously varying through the domain of interest. Such problems have been analyzed in the past by several analytical techniques, especially asymptotic techniques like, e.g., the Wentzel–Kramers–Brillouin (WKB) method, when the profile does not allow analytical solutions. In this work, we analyze the same problem under a purely numerical standpoint, by introducing an advanced adaptive algorithm suitable for the transient analysis of 1-D field propagation in arbitrarily tapered TLs. In the seek for generality, we further extend the TL analogy to general types of nonuniform multiconductor TLs (NMTLs), loaded with general possibly nonlinear and dynamic termination networks. This problem is of extreme relevance in modeling electrical interconnects.

The simulation of electrical interconnects has become an extremely important step for the analysis and design of electronic systems. In fact, as the clock frequencies of digital systems increase, structures usually modeled with lumped elements are no longer electrically small and must be treated as distributed circuits. Parasitic effects like crosstalk and EM coupling cannot be disregarded anymore, because they can seriously affect the overall performance of the system. This is especially relevant for electrical interconnects, which provide the basic link between different devices, parts of a system, or even different systems.

The multiconductor TLs (MTL) model [22] is commonly used for the simulation of practical interconnects. This model assumes a small cross section with respect to the smallest wavelength in the system and quasi-TEM fields in the surrounding of the structure. This is true when the cross section is translation invariant in the direction of propagation of the signals. However, many interconnections of practical interest are characterized by cross sections that are not translation invariant. Examples can be impedance matching networks or cables in complex structures, like automobiles or airplanes. In these cases, the MTL model is not appropriate. However, as long as the cross section remains electrically small, the electric and magnetic fields can be assumed to have a dominant transversal component, i.e., satisfy the quasi-TEM mode of propagation [12]. In this case, the nonuniform multiconductor TLs (NMTL) model can be used to predict the electrical behavior of the interconnect. This model introduces a longitudinal variation in the per-unit-length parameters, by leaving the structure of the equations unchanged. Consequently, the solution of typical nonuniform interconnects does not require a full-wave transient simulation through complex three-dimensional (3-D) EM solvers, which are extremely heavy under a computational standpoint.

Several techniques have been presented for the simulation of the NMTLs. These techniques can be subdivided in two main classes, performing simulation in the frequency domain or in the time domain, respectively. The former can obtain closed-form solutions [2] in some cases, but can also be used to analyze more general structures through a piecewise constant discretization of the line [3]. If the transient response is wanted, inverse fast Fourier transform (FFT) can be used. However, this technique does not allow a true transient simulation, because FFT can only be used to obtain a steady-state solution. The total simulation time must be long enough for the transients to be extinguished. Therefore, when signals with complex waveforms are applied to unmatched lines and long transients are generated, the number of points for the evaluation of the FFT can be very large. In addition, nonlinear terminations cannot be handled with this approach. These are the reasons why numerical schemes performing the simulation directly in the time domain have been recently proposed. Among these we can cite the methods based on the scattering representation [10], the method of characteristics

Manuscript received August 30, 1999; revised July 14, 2000.

The author is with the Dipartimento di Elettronica, Politecnico di Torino, 10129 Torino, Italy(e-mail: grivet@polito.it).

Publisher Item Identifier S 0018-926X(00)09358-3.

0018–926X/00$10.00 © 2000 IEEE

[26], spectral methods [21], and the waveform relaxation analysis [5]. Several other schemes are available for uniform MTL simulation, such as the common finite-difference time-domain (FDTD) scheme.

This work presents a new time-space adaptive scheme for the transient simulation of nonuniform interconnects. The terminations can be arbitrary, including nonlinear and dynamic networks. The scheme uses biorthogonal wavelet bases both to expand the voltages and currents along the line and to test the NMTL equations. The intrinsic multiresolution properties of wavelet approximations make it possible to carefully select a minimal number of unknowns to construct a highly sparse yet accurate representation of the solution at each time step. It will be shown that this can be obtained in a straightforward way through absolute thresholding of the wavelet coefficients. In addition, it will be shown that the space-adaptive approximation can be easily modified in time in order to track the fine structures of the solution as they move and change shape during the simulation. The finite propagation speed will play a crucial role in this respect. A set of numerical results will prove the high degree of adaptivity that can be achieved by the proposed algorithm.

The multiresolution properties of wavelets are well known in various electrical engineering fields, ranging from signal processing and data compression to sparsification and preconditioning of matrices stemming from method of moments (MoM) discretizations. Recently, they have been used to construct so-called multiresolution time-domain (MRTD) schemes, which have been shown to present some advantages with respect to more standard FDTD schemes for time-domain EM modeling [19], [20], [23], [25]. This paper proposes a discretization scheme that also tries to overcome, through use of wavelets, the limitations of FDTD, namely limited accuracy, large computation times and memory occupation. Multiresolution (wavelet) bases seem to be very promising, since they provide optimal representations of the fields. However, the construction of wavelet-based discretizations with a robustness and flexibility comparable to FDTD is still a challenging task. Nonetheless, this paper shows that wavelets can be used in a very effective way to achieve time-space adaptivity, allowing time-dependent mesh generation and refinement by means of simple algorithms (see also [11], [12], and [14]).

Here follows an outline of this work. Section I introduces the equations that will be solved. Section II describes the general discretization scheme based on a weak formulation of the NMTL equations. The trial and test functions are then defined in Section III, which describes the basic properties of wavelets allowing for space adaptivity. Section IV details the accuracy of the scheme and the algorithm leading to time-space adaptivity. Finally, numerical results are presented in Section V.

II. Problem Statement

Under the quasi-TEM assumption any interconnect may be described through the NMTL equations [22]

$$\frac{\partial}{\partial z}\mathbf{v}(z,t)+\mathbf{L}(z)\frac{\partial}{\partial t}\mathbf{i}(z,t)+\mathbf{R}(z)\mathbf{i}(z,t)=0 \qquad (1)$$

$$\frac{\partial}{\partial z}\mathbf{i}(z,t)+\mathbf{C}(z)\frac{\partial}{\partial t}\mathbf{v}(z,t)+\mathbf{G}(z)\mathbf{v}(z,t)=0 \qquad (2)$$

with $\mathbf{v}(z,t)$ and $\mathbf{i}(z,t)$ indicating the voltage and current vectors at location z and time t. The line is assumed to have $P+1$ conductors, labeled with $i=0,\ldots,P$, with the zeroth taken as the reference for voltages and the return for currents. The per-unit-length parameters $\mathbf{L}(z)$, $\mathbf{C}(z)$, $\mathbf{R}(z)$, and $\mathbf{G}(z)$ are $P\times P$ matrices whose entries are arbitrary functions of the space variable z. We will consider the length of the line to be normalized. The change of variable $z=\mathcal{L}\varsigma$ can be used for lines of length $\mathcal{L}$, with $\varsigma\in[0,1]$. However, hereafter we proceed using z without loss of generality.

It will be convenient in the following to consider a form of the NMTL equations that is explicit in the time derivatives. Therefore, we restate the NMTL equations as

$$\frac{\partial}{\partial t}\mathbf{i}(z,t)=-\mathbf{\Gamma}(z)\frac{\partial}{\partial z}\mathbf{v}(z,t)-\mathbf{\Gamma}(z)\mathbf{R}(z)\mathbf{i}(z,t) \qquad (3)$$

$$\frac{\partial}{\partial t}\mathbf{v}(z,t)=-\mathbf{S}(z)\frac{\partial}{\partial z}\mathbf{i}(z,t)-\mathbf{S}(z)\mathbf{G}(z)\mathbf{v}(z,t) \qquad (4)$$

where $\mathbf{S}(z)=\mathbf{C}(z)^{-1}$ and $\mathbf{\Gamma}(z)=\mathbf{L}(z)^{-1}$.

The line terminations will be modeled as arbitrary nonlinear and dynamic voltage-controlled multiports, described by their state equations. This model is derived from general electrical network theory [1]. More precisely, the termination at $z=0$ will be characterized by

$$\begin{aligned}\frac{d}{dt}\mathbf{x}_0(t)&=\mathbf{f}_0(\mathbf{x}_0(t),\mathbf{v}(0,t),\mathbf{u}_0(t);t)\\ \mathbf{i}(0,t)&=\mathbf{g}_0\left(\mathbf{x}_0(t),\mathbf{v}(0,t),\mathbf{u}_0(t),\frac{d}{dt}\mathbf{u}_0(t);t\right)\\ &\quad+\mathbf{Q}_0\frac{d}{dt}\mathbf{v}(0,t)\end{aligned} \qquad (5)$$

where

- $\mathbf{x}_0$ state-variable vector;
- $\mathbf{u}_0$ vector including the independent sources;
- $\mathbf{f}_0,\mathbf{g}_0$ nonlinear functions.

The matrix $\mathbf{Q}_0$ allows to include the effect of lumped shunt capacitors. A similar model is considered for the termination network at $z=1$, for which the suffix $_1$ is used. It should be noted that the model for the termination networks herewith considered includes the case of linear loads, which can be recovered by setting the functions $\mathbf{f}$ and $\mathbf{g}$ to be linear. The case of static terminations is an obvious particular case with no state variables and with a vanishing matrix $\mathbf{Q}$.

III. Weak Formulation of NMTL Equations

The true solution of (3) and (4) loaded with (5) lies in some functional space $\mathcal{S}$. A numerical approximation will be sought for in some finite dimensional approximation space $\mathcal{S}_h\subset\mathcal{S}$ such that $\mathcal{S}_h\to\mathcal{S}, h\to 0$. This condition insures the consistence of the discretization as the parameter h vanishes. As for the solution vectors, also the per unit length parameters will be assumed to belong to some functional space $\mathcal{P}$, which can be approximated by some spaces $\mathcal{P}_h\subset\mathcal{P}$ with the same convergence properties, $\mathcal{P}_h\to\mathcal{P}, h\to 0$. The approximation of

the per-unit-length parameters does not constitute a numerical problem since the quasi-TEM assumption requires their longitudinal variations to be small. On the other hand, this approximation simplifies the construction of the discrete system to be derived in the following (see Appendix A).

We introduce now two sets of basis functions for the approximation spaces

$$\mathcal{S}_h = \text{span}\{\xi_n, n = 1, \ldots, N_\xi\} \tag{6}$$

$$\mathcal{P}_h = \text{span}\{\phi_k, k = 1, \ldots, N_\phi\} \tag{7}$$

where N_ξ and N_ϕ must be finite and are dependent on the discretization parameter h. The voltage and current vectors can be expanded into these basis functions

$$\mathbf{v}(z,t) = \sum_{n=1}^{N_\xi} \xi_n(z)\mathbf{v}_n(t)$$

$$\mathbf{i}(z,t) = \sum_{n=1}^{N_\xi} \xi_n(z)\mathbf{i}_n(t)$$

as well as the per-unit-length parameters $\mathbf{\Gamma} = \sum_{k=1}^{N_\phi} \phi_k(z)\mathbf{\Gamma}_k$ and similarly for the other matrices. We introduce also a third set of functions, which will be taken as test functions for the derivation of a weak form of the NMTL equations. The only restriction on these functions denoted as $\{\eta_m,\ m = 1, \ldots, N_\xi\}$ is that they are linearly independent. If we substitute the above expansions in the NMTL equation (3) and (4) and take the inner product of the resulting expressions with each η_m, we get a system of ordinary differential equations (ODEs), where the expansion coefficients $\mathbf{v}_n(t)$ and $\mathbf{i}_n(t)$ are the unknowns. The equations of the terminations can be combined with this system by eliminating the border current coefficients $\mathbf{i}_1$ and $\mathbf{i}_N$ in terms of the voltage coefficients $\mathbf{v}_1$ and $\mathbf{v}_N$ and of the state variables $\mathbf{x}_0, \mathbf{x}_1$. This procedure involves a straightforward substitution and is not further detailed here. Some remarks on stability are given in Appendix B. The result is a global system of ordinary differential equations which reads

$$\mathbf{\Psi}\frac{d}{dt}\mathbf{y}(t) = \mathbf{\Phi}\mathbf{y}(t) + \mathcal{F}(\mathbf{y}(t)) \tag{8}$$

where the vector $\mathbf{y}$ includes the expansion coefficients of voltages and currents as well as the state-variable vectors of the terminations, the matrices $\mathbf{\Psi}$, and $\mathbf{\Phi}$ are highly sparse and the nonlinear function $\mathcal{F}$ involves only the few border coefficients and the state variables of the termination networks.

It was shown in [13] that when the trial and test functions constitute biorthogonal sets, the matrix $\mathbf{\Psi}$ reduces to the identity. This is not true if more traditional functions like, e.g., triangle functions or higher order finite-element functions, are used in a Galerkin scheme. The bases that we will use in this work are indeed pairs of biorthogonal systems, and will lead to a fully explicit system of ODEs (i.e., $\mathbf{\Psi} = \mathcal{I}$). The advantage lies in the fact that the system (8) becomes explicit in the time derivatives and can be inserted in a suitable time-stepping algorithm that does not require the inversion of any matrix at each time iteration.

IV. Sparse Wavelet-Based Biorthogonal Discretization

This section details the construction of sparse approximations based on biorthogonal systems of wavelets defined on the interval. Since wavelet theory is well established we will recall only the specific properties of wavelets that are of relevance for this work. For further details we recommend the many books and papers already available on the subject (see, e.g., [6], [8], [15]).

Let us consider a function $v \in L^2$ defined on a domain $\Omega \subseteq \mathbf{R}$. We want to approximate v by performing its projection onto a suitable finite-dimensional space V_J, with the refinement level J controlling the accuracy of the approximation. Wavelet theory shows that once a coarse level $j_0 < J$ is defined, the two following alternative representations hold:

$$v(z) \simeq \sum_k c_{J,k}\varphi_{J,k}(z) \tag{9}$$

$$v(z) \simeq \sum_k c_{j_0,k}\varphi_{j_0,k}(z) + \sum_{j=j_0}^{J-1}\sum_k w_{jk}\psi_{jk}(z). \tag{10}$$

The first representation is called *canonical*, because it is the usual form in which finite element approximations are expressed. For example, one could replace the scaling functions $\varphi_{J,k}$ with triangle functions (or, equivalently, linear finite elements), and the coefficients $c_{J,k}$ would be the nodal values of the original function v. The second representation is called *hierarchical*, because it involves the iterative superposition of details through superposition of wavelets ψ_{jk} at increasing levels j, without modifications of the coarser parts of the approximation. Convergence in L^2 sense is guaranteed as $J \to \infty$.

The main advantage in the hierarchical decomposition is that the wavelets ψ_{jk} can be designed to be extremely localized in space around the points $z_{jk} = (k+0.5)\,2^{-j}$, with a support proportional to 2^{-j}. If the function v to be approximated is characterized by a small region with fast variations and is smooth elsewhere, it can be shown that only a small portion of the coefficients w_{jk} should be retained. In addition, the location and the number of needed details can be automatically determined by looking at the magnitude of the wavelet expansion coefficients. This leads to extremely sparse representations, which can be *adapted* to the function v being analyzed. More precisely, the adapted sparse representation can be defined as

$$v(z) \simeq \sum_k c_{j_0,k}\varphi_{j_0,k}(z) + \sum_{(j,k)\in\Lambda_\epsilon} w_{jk}\psi_{jk}(z) \tag{11}$$

where

$$\Lambda_\epsilon = \{(j,k) : |w_{jk}| > \epsilon\} \tag{12}$$

and ϵ is a threshold controlling the accuracy/sparseness of the approximation. The optimality of such representations in terms of norm of the approximation error in general Sobolev or Besov spaces is a well-known fact in wavelet theory [9] and is not recalled here. Examples of the high degree of sparsity that can be achieved with adapted representations of typical signals in electrical interconnects can be found in [11] and in Section VI.

The wavelets employed in this work are biorthogonal B-splines wavelets. We prefer biorthogonal instead of orthogonal systems like, e.g., Battle–Lemariè or Haar wavelets, since we want to preserve regularity, small compact support, and symmetry of the basis functions around their center z_{jk}. These three requirements are not compatible in orthogonal settings [8]. We will use in particular the B-splines $(2,2)$ system, constructed from piecewise linear B-splines and characterized by two vanishing moments for both primal and dual wavelets. This system is quite convenient since the primal scaling functions are triangle functions, i.e., are equivalent to standard 1-D finite elements, while the dual scaling functions are those with smallest possible support among all B-splines duals [6].

The domain of interest is necessarily bounded since the length of the TL is finite. Therefore, it is necessary to consider special wavelet systems defined on bounded domains. It is clear that these cannot be constructed through translations and dilations of a single function as in infinite or circular domains. The construction of wavelet systems on bounded domains is usually based on the modification of the few functions having support crossing the edges of the domain. This is not a trivial task if a good localization of the border functions is to be preserved, which is essential for this work. For this reason, we employ the special construction derived in [15], specifically developed in order to optimize localization at the edges and, of course, preserving polynomial exactness, vanishing moments, stability, and biorthogonality. One additional feature of this construction is the so-called *boundary adaption*, consisting of only one nonvanishing wavelet per refinement level when evaluated at the borders. This fact is quite convenient for the implementation of the boundary conditions.

Given the biorthogonal B-splines $(2,2)$ system, we use the primal scaling functions and wavelets for expansion of voltages and currents along the TL and the corresponding duals for testing the NMTL equations in order to derive a discrete system of ODEs. It is well known [6], [15] that the dual scaling functions and wavelets are not defined in closed form but only through iterative refinement equations. In addition, they are poorly regular. These two facts make the computation of the testing integrals a difficult task since no quadrature formulas can be used efficiently. However, there exist alternative formulations [7] allowing to restate these integrals as eigenvector problems associated to special matrices derived from the scaling functions filters. Further details are found in Appendix A.

V. Accuracy, Time Discretization, and Adaptivity

We discuss in this section the main features of the proposed algorithm. First, the spatial accuracy of the discretization is investigated. This will help in determining which particular time-stepping scheme is most suitable for the present application. Then, the dynamic time–space adaptive strategy leading to sparse iterations is detailed and discussed.

Let us consider the spatial differentiation operator $\partial/\partial z$ acting on a generic function $v(z)$ and derive its weak approximation through expansion of v into the set of scaling functions

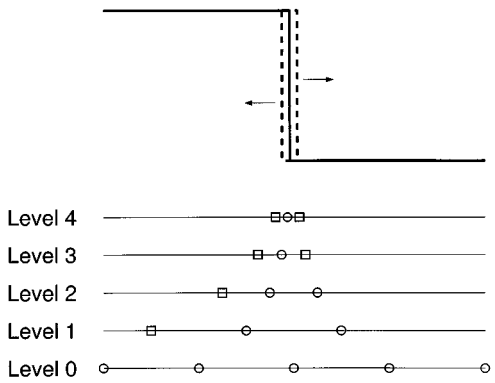

Fig. 1. Generation of the set of active indexes $\hat{\Lambda}_c^{n+1}$ at time $n+1$ from the set of active indexes Λ_c^n at time n (circles). The set $\hat{\Lambda}_c^{n+1}$ is generated from Λ_c^n by adding one coefficient on the left and one on the right per refinement level j. The added coefficients (squares) allow to capture both forward and backward propagation (dashed lines) of a singularity (continuous line).

$\varphi_{J,k}$ (see (9)) and testing with the corresponding duals $\tilde{\varphi}_{J,k}$. In the biorthogonal B-splines $(2,2)$ case we get

$$\left\langle \tilde{\varphi}_{J,k}, \frac{\partial}{\partial z} v \right\rangle = \frac{1}{12\Delta z}(c_{J,k-2} - 8c_{J,k-1} + 8c_{J,k+1} - c_{J,k+2}) \qquad (13)$$

for any k, where $\Delta z = 2^{-J}$ is the spatial resolution of the approximation. The right-hand side of this expression is a stencil to be applied to the sequence of expansion coefficients $c_{J,k}$ in order to perform differentiation. This is easily recognized as the same stencil of a centered explicit fourth-order finite-difference scheme [11], [17]. This proves that the order of consistency of the discretization is four, even if the trial functions are only piecewise linear. In other words, there is a superconvergence effect intrinsic in the discretization process. In addition, since there is a full equivalence between the canonical and the hierarchical representations of (9) and (10), we are led to the conclusion that also the multiresolution discretization using wavelets is fourth-order accurate in space.

Given this equivalence, it is necessary to select a proper time integration method in order to exploit the advantages of the high spatial accuracy and to insure time stability. If a standard leapfrog scheme is used, we only get second order accuracy in time. Moreover, it can be shown [17] that the stability limit for leapfrog in time with fourth-order differencing in space is $\Delta t \leq 0.72\Delta z/v_{\max}$, i.e., the time step must be smaller than the Courant condition for standard FDTD. For this reason we are led to choose another possibly high-order time integration scheme that is capable of preserving stability with a larger Courant number. We found that a good choice is a fourth-order Runge–Kutta scheme [17]. In fact, the accuracy of this time discretization matches the accuracy of the spatial discretization, which is desirable for hyperbolic equations, and in addition the stability limit requires only the time step to satisfy $\Delta t \leq 2.06\Delta z/v_{\max}$. More details on stability are given in Appendix B. A further advantage is that the dispersion errors are quite insensitive to the specific Courant number at

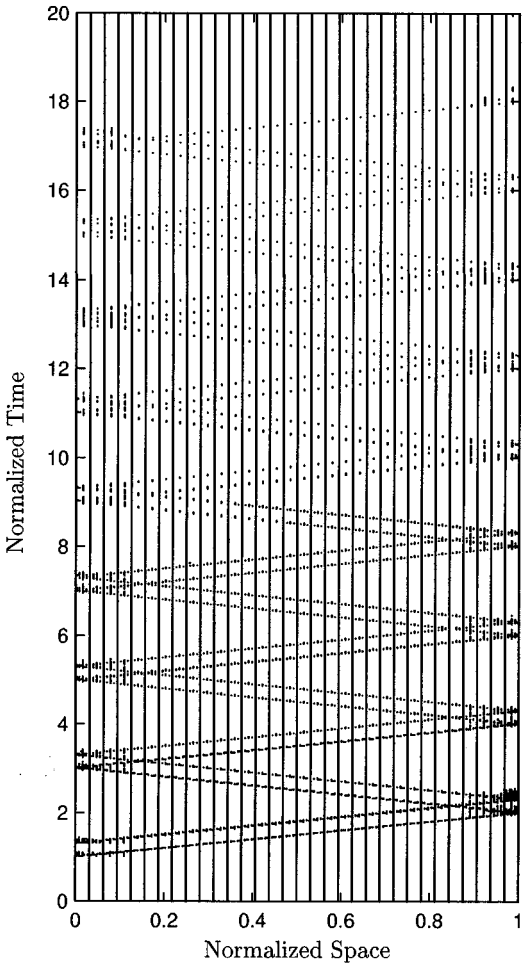

Fig. 2. Adaptive solution for an unmatched lossless scalar line. The dots represent the location of the active wavelet coefficients automatically selected by the adaptive algorithm to compute the solution.

which the scheme is run. This means that all different modes of arbitrary multiconductor lines characterized by different modal velocities will be affected by approximately the same dispersion errors [16].

Once the time discretization has been performed, the fully discrete system reads

$$\mathbf{y}^{n+1} = \mathcal{H}(\mathbf{y}^n) \tag{14}$$

where the superscript n denotes the time iteration corresponding to time $t^n = n\Delta t$. Due to the structure of (8), the operator $\mathcal{H}$ is linear and sparse for most of the unknowns, and presents a nonlinear part involving only the few coefficients related to the border basis functions, as well as the state variables of the termination networks. When all coefficients are retained in the spatial approximation, the scheme is equivalent to a nonadaptive fourth-order finite difference scheme with fourth-order Runge–Kutta time stepping.

We consider now the improvement of the scheme through implementation of a dynamic adaptive strategy, in order to exploit the sparsity of wavelet-based approximations. To this end, we consider the system of type (14) obtained using the hierarchical representation (10) to approximate the unknown voltage and current waveforms along the line. At any fixed time t_n, the array $\mathbf{y}^n$ includes all the expansion coefficients into scaling functions at the coarse level j_0 plus all the expansion coefficients into wavelets at increasing levels $j = j_0, \ldots, J-1$. Let us fix now an absolute threshold ϵ and consider the sparse approximation obtained by neglecting all wavelet coefficients smaller than ϵ, according to (11) and (12). The remaining "active" coefficients, which correspond to a set of indexes $(j,k) \in \Lambda_\epsilon^n$, are collected in the array denoted as $\mathbf{y}^n\{\Lambda_\epsilon^n\}$. The length of this array may be much smaller than the total number of coefficients for typical waveforms, as shown in the numerical results of Section V. More precisely, we have

$$\#\{\Lambda_\epsilon^n\} \ll \#\{\Lambda_{\epsilon=0}^n\}.$$

This happens especially when there are localized regions of fast variations embedded in regions of smoothness, like in the case of Gaussian pulses or step functions with fast rise times. It is important to note that all the information needed to compute the solution (with accuracy/sparsity controlled by the threshold ϵ) at the next time iteration through (14) is available in $\mathbf{y}^n\{\Lambda_\epsilon^n\}$.

The algorithm becomes fully adaptive if we manage to guess which will be at the next time iteration $n+1$ the set of "active" coefficients Λ_ϵ^{n+1}. In fact, it is clear that this set depends on the specific time iteration since it is determined from the actual structure of the solution along the line. In other words, we need an operator $\mathcal{E}$ acting on sets of indexes so that

$$\Lambda_\epsilon^{n+1} = \mathcal{E}(\Lambda_\epsilon^n).$$

If this operator is known, we will be able to compute directly only a subset of coefficients $\mathbf{y}^{n+1}\{\Lambda_\epsilon^{n+1}\}$ that will correspond to the active coefficients at iteration $n+1$, being sure that the other coefficients will be smaller than the threshold ϵ and, thus, nonsignificant. Even if this operator may seem difficult to characterize, its structure is easily determined by the dynamics of the TL equations. Indeed, these equations support bidirectional propagation at a maximum speed $v_{\max}$. Therefore, if there is a region with fast variations centered at z_0, we are sure that this region will not be able to move within a time step of width Δt outside the interval $[z_0 - v_{\max}\Delta t, z_0 + v_{\max}\Delta t]$. We know that a localized singularity remains localized at the next time iteration and we know exactly where this singularity will be located. The only missing information is the direction of propagation, which can be either forward or backward. The above considerations give a simple rule to determine a first guess $\hat{\Lambda}_\epsilon^{n+1}$. This is generated by simply adding one coefficient on the left and one coefficient on the right of existing coefficients in the set Λ_ϵ^n for each refinement level j. This procedure is depicted in Fig. 1. The obvious condition under which this strategy is effective is that the Courant number be not larger than one. In fact, if $\Delta t > \Delta z / v_{\max}$, more than one additional coefficient may be necessary, resulting in reduced sparsity and increased computational complexity. Therefore, from now on, we will restrict the Courant number to be at most equal to one. This requirement is compatible with the stability requirements discussed above. At this point, the time iteration from n to $n+1$ can be performed by computing only a subset of coefficients. The other coefficients will be smaller than the threshold ϵ and thus non significant.

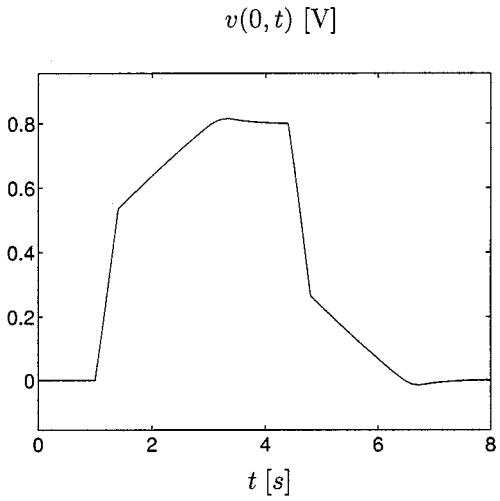

(a)

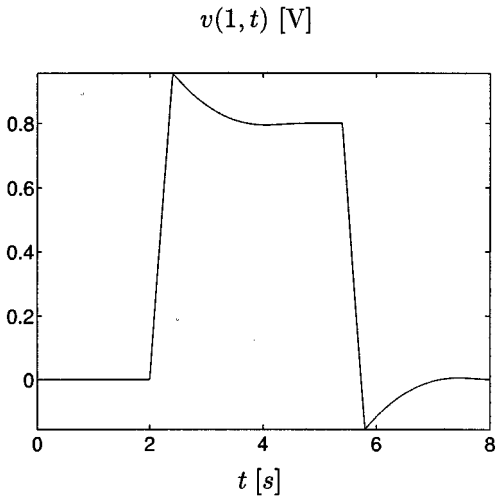

(b)

Fig. 3. Solution for the matched 1 : 4 exponential line excited by a trapezoidal pulse voltage source. Voltages at the (a) left and (b) right terminations.

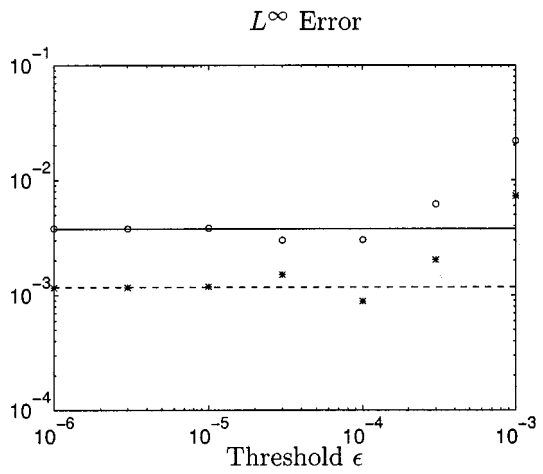

(a)

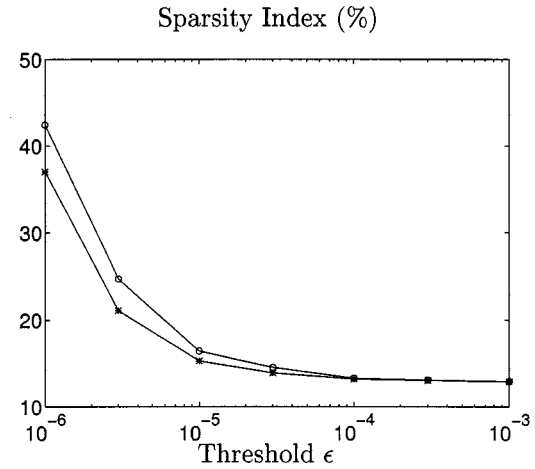

(b)

Fig. 4. Matched 1 : 4 exponential line with trapezoidal voltage source. (a) Maximum absolute error on voltage (circles) and current (stars) obtained with the adaptive scheme as a function of the threshold ϵ used for the wavelet coefficients. The solid and dashed lines indicate the approximation errors obtained with no wavelet thresholding for voltage and current, respectively. (b) Sparsity index of the adaptive approximation as a function of the threshold ϵ.

Once the solution $\mathbf{y}^{n+1}\{\hat{\Lambda}_\epsilon^{n+1}\}$ has been computed, the true set of active indexes Λ_ϵ^{n+1} is obtained through thresholding of the (few) wavelet coefficients indexed by $\hat{\Lambda}_\epsilon^{n+1}$. We summarize in the following list the simple steps to be performed by the adaptive algorithm at each time iteration.

1) For each level j perform absolute thresholding, i.e., define an array of unknowns including all the state variables, all the scaling function coefficients at the coarse level j_0 and only the wavelet coefficients with magnitude larger than the threshold ϵ; denote the corresponding set of indexes as Λ_ϵ^n.
2) For each level j extend the set of "active" coefficients by one on the left and on the right, in order to capture propagation in either direction (which is not known *a priori*); denote this set of indexes as $\hat{\Lambda}_\epsilon^{n+1}$.
3) Apply the iteration operator (14) restricted to the index sets just determined. In compact notations

$$\mathbf{y}^{n+1}\left\{\hat{\Lambda}_\epsilon^{n+1}\right\} = \mathcal{H}\left(\mathbf{y}^n\left\{\Lambda_\epsilon^n\right\}\right).$$

4) Go back to step 1) to perform the next time iteration.

We remark that the thresholding procedure removes energy (associated to the details that can be neglected at no loss of accuracy) from the waveforms at each time iteration and, therefore, has no effect on the time stability of the scheme.

VI. Numerical Results

We present in this section several numerical examples illustrating and validating the proposed adaptive scheme. The first case to be analyzed consists of a scalar uniform lossless TL with normalized parameters (characteristic impedance $Z_c = 1$, and one-way delay time $T = 1$). The line is excited by a trapezoidal step-voltage source with finite rise time $\tau = 0.3T$ and internal resistance $R_S = 0.1\ Z_c$, and loaded by a resistance $R_L = 10\ Z_c$. The analytical solution to this simple problem is well known. However, this represents a good canonical test case for the adaptive algorithm since we are using a forcing function with regions of fast variations and since the pulse undergoes significant reflections at the terminations during its propagation. Fig. 2 represents the outcome of the adaptive algorithm. Each

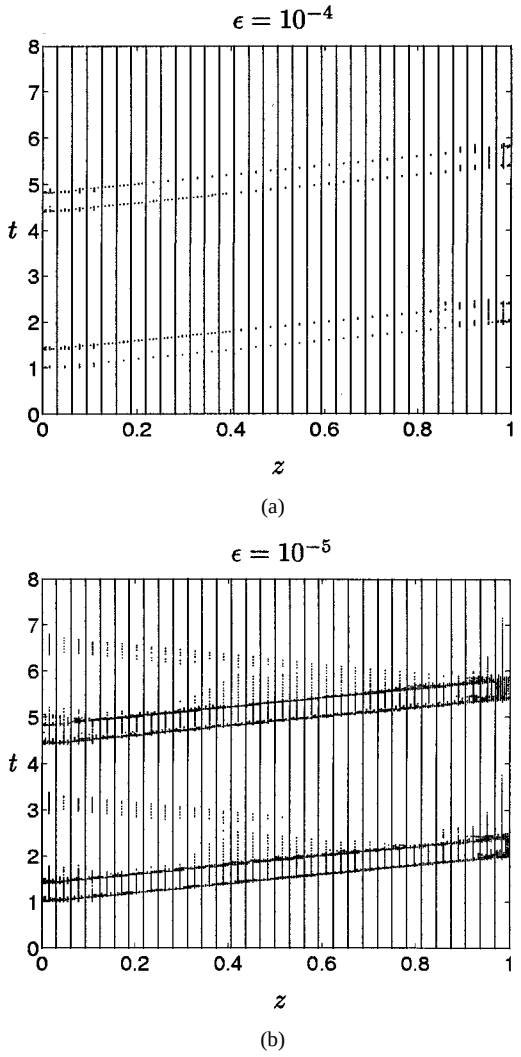

Fig. 5. Location of the active voltage wavelet coefficients larger than (a) $\epsilon = 10^{-4}$ and (b) $\epsilon = 10^{-5}$.

dot in the plot represents the location z_{jk} of an active wavelet coefficient automatically detected by the algorithm to be larger than the threshold $\epsilon = 10^{-5}$ and consequently used for the computations. It can be clearly seen from the figure that the active coefficients crowd along the characteristic curves of the TL equation that correspond to the regions of fast variations in the solution. As time progresses, the amplitude of the reflected waves dims to zero, and the corresponding adaptive representation needs less and less details to approximate it. This is the reason why the density of the active coefficients diminishes as the pulse is successively reflected. These results confirm the high adaptivity guaranteed by the wavelet-based representation.

In order to quantify the degree of adaptivity and its dependence on the cutoff threshold ϵ, we performed a study on a nonuniform line whose solution is known analytically, the exponential line [4]. This line is characterized by exponentially tapered per-unit-length inductance and capacitance

$$L(z) = L^0 e^{\delta z}, \quad C(z) = C^0 e^{-\delta z}$$

where the parameter δ controls the rate of taper and L^0, C^0 are the nominal per unit length inductance and capacitance at the

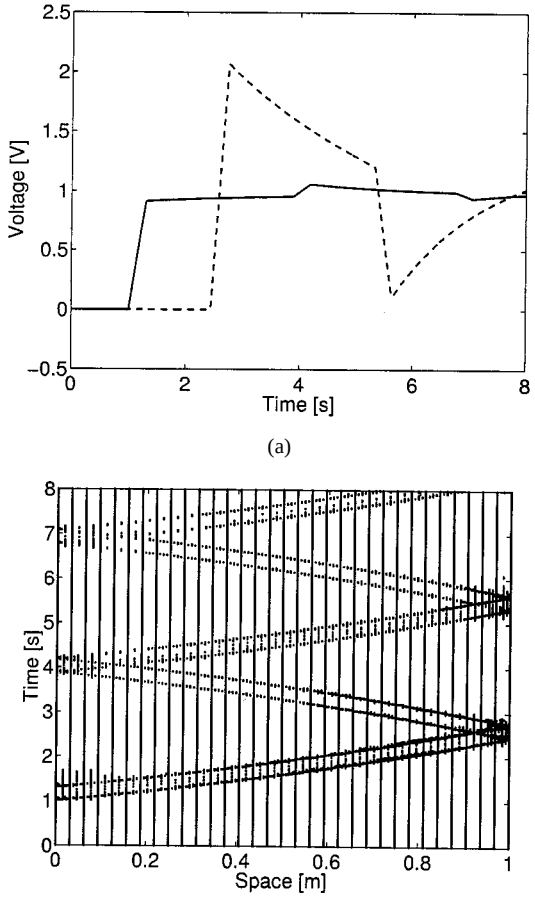

Fig. 6. (a) Voltage at the left (solid line) and right (dashed line) terminations of a line with exponentially decreasing phase speed. (b) Location of the active voltage wavelet coefficients.

edge $z = 0$. The nominal characteristic impedance of the line is, therefore

$$Z_c(z) = \sqrt{\frac{L(z)}{C(z)}} = Z_c^0 e^{\delta z}.$$

The parameters of the line that are used here are $L^0 = 1$ H/m, $C^0 = 1$ F/m, and $\delta = \log 4$, corresponding to a $1:4$ impedance stepping line with unitary delay time $T = 1$ s. The terminations are matched, and the line is excited by a trapezoidal pulse voltage source (rise time $\tau_r = 0.4$ T, duration $\tau = 3.4$ T). The analytical solution is computed in the frequency domain and inverse FFT is used to recover the time domain response. The exact voltages at the left and right terminations are depicted in Fig. 3.

The same structure has been solved with the proposed wavelet-based adaptive algorithm by setting the maximum allowable refinement level to $J = 8$. Fig. 4(a) reports the approximation errors on voltage and current obtained with wavelet thresholding for different values of the threshold ϵ. The error is here defined in L^∞ norm, i.e., represents the maximum absolute deviation in space and time between the exact and the computed solution. Fig. 4(b) reports the sparsity index of the adaptive approximation, defined as the percentage of active coefficients used for the computations with respect to the total

number of coefficients, plotted as a function of the threshold ϵ. Highly sparse representations can be obtained at no loss of accuracy. Indeed, the errors obtained with thresholding are always comparable to the corresponding errors in the solution without thresholding, indicated in Fig. 4(a), with solid (voltage) and dashed (current) lines. Fig. 5 depicts the location of the active wavelet coefficients in the (z,t) plane for two different values of the threshold ϵ. As for the uniform line, these plots give a quick interpretation of the solution in terms of travelling waves, which in this case are not simple translations of a single pulse as the time increases, but are affected by "distributed" reflections due to the nonuniformity of the line.

In order to show the generality and robustness of the proposed scheme, we performed the analysis of a nonuniform line with a nonuniform phase speed. This example could model propagation in media characterized by a continuous variation of the constitutive parameters. The line is characterized as follows. The (normalized) per-unit-length parameters are

$$L(z) = 4^z \text{ H/m}, \quad C(z) = 1 \text{ F/m}.$$

These parameters lead to an exponentially increasing nominal characteristic impedance (from 1Ω up to 2Ω) and to an exponentially decreasing nominal phase speed,

$$\nu(z) = \frac{1}{\sqrt{L(z)C}}.$$

We consider a nonmatched line with nominal reflection coefficients at the left and right ends equal to $\Gamma_S = -9/11$ and $\Gamma_L = 2/3$, respectively. With these load conditions, the input voltage pulse undergoes significant reflections at the line ends. The voltage waveform used in the following is a 1 V step function with rise time equal to 0.3 s. The resulting voltages at the left and right terminations are plotted in Fig. 6(a), while the location of the active wavelet coefficients (using a threshold $\epsilon = 10^{-4}$) are plotted in Fig. 6(b). It should be noted that these coefficients follow the characteristic curves of the TL equations, tracking the location of the singularities (i.e., the points where the derivative of voltage and current is discontinuous). These curves are significantly bent, with a tangent at a fixed z equal to $\pm 1/\nu(z)$. The figure clearly shows the sparsity in the overall representation of the solution and the high adaptivity of the method.

We proceed now with two examples of lines with nonlinear and dynamic terminations. The first is a uniform scalar TL with normalized characteristic impedance and delay time $(Z_0 = 1, T = 1)$ excited by a unitary step generator with rise time $\tau = 0.3T$ and unitary internal resistance and loaded with a capacitor $(C = 1)$ and a diode in parallel. We chose this simple validation example because it can be readily analyzed with SPICE. Fig. 7(a) shows the voltages at the two line terminations, indicating excellent agreement between the wavelet and the SPICE simulations. Fig. 7(b) shows the location in the $[z,t]$ plane of the active wavelet coefficients actually used for the computations. Also in this case, it can be noted that very few coefficients are needed and that these coefficients are located around the characteristic curves along which the fast variations of the solution occur.

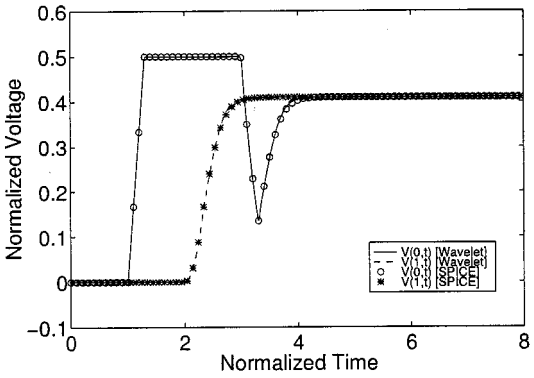

(a)

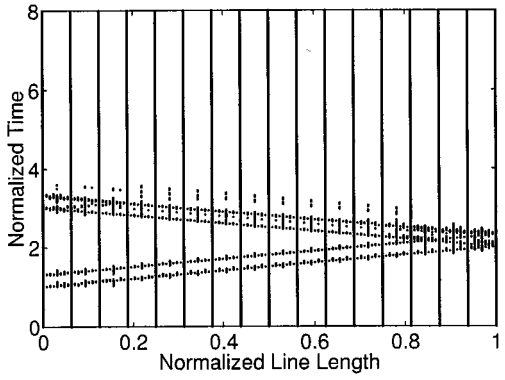

(b)

Fig. 7. (a) Normalized voltages at the terminations of a scalar TL excited by a step generator and loaded with a capacitor and a diode. (b) Locations of the significant voltage wavelet coefficients actually used for the computation of the solution.

The second example is a more realistic structure, depicted in Fig. 8. It consists of two nonparallel PCB lands over a reference ground plane. The voltage pulse $v_s(t)$ is a 5 V step with rise time $\tau = 200$ ps. The cross section of the interconnect is electrically small throughout the significant frequency spectrum of this waveform, therefore, a quasi-TEM propagation of the fields can be assumed and (1) and (2) are valid (see [12]). The crosstalk voltages at the left and right terminations are reported in Fig. 9(a), while the locations of the active voltage wavelet coefficients are reported in Fig. 9(b). Also in this case the solution was computed by using very few coefficients.

VII. Conclusion

A discretization scheme for the transient simulation of NMTLs loaded with arbitrary nonlinear and dynamic networks has been presented. The scheme is based on a weak formulation of the equations employing biorthogonal wavelet systems as trial and test functions. The particular wavelet bases employed in this work, namely biorthogonal piecewise linear B-spline wavelets, leads to a fourth-order scheme in both space and time. The key advantage of this formulation lies in the possibility of adaptively selecting a minimal number of basis functions

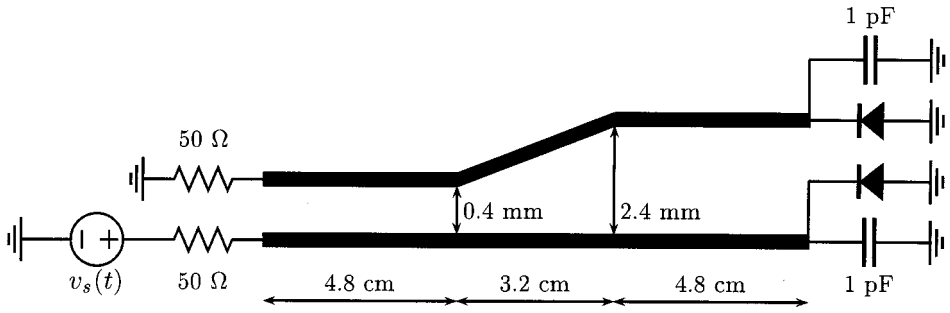

Fig. 8. Typical printed circuit board (PCB) configuration (top view) with nonparallel traces and termination networks. The width of the traces is 0.2 mm. The structure is above a reference ground plane and a dielectric substrate 0.6 mm high with $\varepsilon_r = 4.7$.

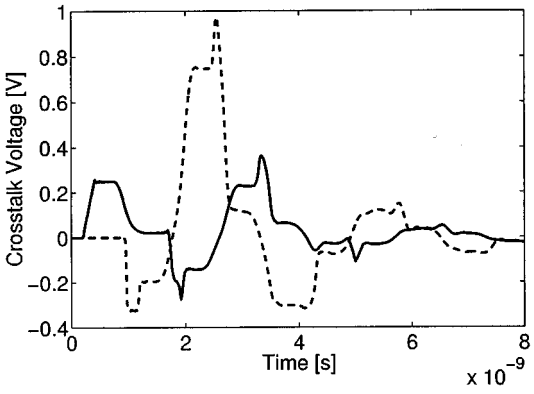

(a)

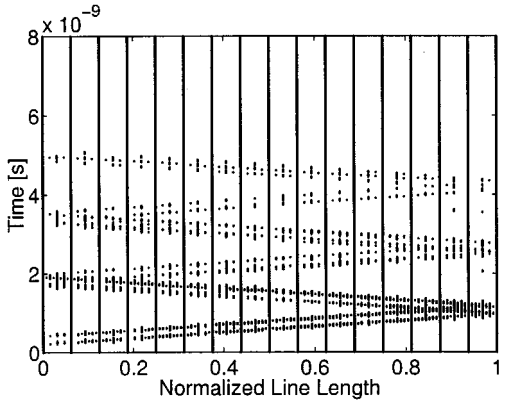

(b)

Fig. 9. (a) Crosstalk voltages at the left (continuous line) and right (dashed line) terminations of the interconnect of Fig. 8. (b) Locations of the active voltage wavelet coefficients actually used for the computations.

to represent the solution at each time iteration. The intrinsic hierarchical nature of wavelet approximations leads indeed to a very sparse representation of the solution at each time step, thus allowing computations through a time–space adaptive discretization. The presented numerical examples demonstrate the high degree of adaptivity exploited by the proposed algorithm. As a consequence, the scheme allows significant savings of memory occupation and computing time with respect to more standard nonadaptive discretization schemes. Further research is in progress to extend the algorithm to transient EM field computations in higher dimensions as well as more complicated geometries.

Appendix A
Integrals of Wavelets

Here we will show how integrals involving products of scaling functions and wavelets can be computed at machine precision without the need of any quadrature formula. The original formulation with the related mathematical proofs can be found in [7]. The key fact allowing for this procedure is the presence in the integrals of only refinable functions or their derivatives. All scaling functions and wavelets including duals satisfy indeed a refinement equation [6], [8].

The general form of the testing integrals needed for the discretization of the NMTL equations can be reduced through successive application of the refinement equations to

$$\mathbf{I}(\alpha_1, \ldots, \alpha_m) = \int \Upsilon^0(z) \prod_{m=1}^{M} D^{\mu_m} \Upsilon^m(z - \alpha_m)\, dz \quad (15)$$

where D is the spatial differentiation operator, $\mu_m = \{0, 1\}$, and α_m are integers for any value of m. The functions Υ^m can be either equal to φ or $\tilde{\varphi}$, while Υ^0 is the Haar scaling function. Note that this procedure is possible only if the per-unit-length parameters are expanded into a set of refinable functions, e.g., $\phi_k = \varphi_k$ in (7). This is the reason why the approximation of the per-unit-length parameters defined in Section II was included in the discretization process.

Due to the properties of the functions in the integrand, it can be shown that also the multivariate function $\mathbf{I}$ satisfies a vector refinement equation of the type

$$\mathbf{I}(\mathbf{k}) = \sum_{\mathbf{m} \in \mathbb{Z}^M} \mathbf{h}_{\mathbf{2k-m}} \mathbf{I}(\mathbf{m}), \quad \mathbf{k} \in \mathbb{Z}^M. \quad (16)$$

The above relation can be interpreted as an eigenvector problem associated to the eigenvalue $\lambda = 1$. The normalization of the eigenvector depends on the number of differentiations in the integral and is detailed in [7]. The components of this eigenvector coincide with the testing integrals.

Appendix B
Boundary Conditions and Stability

The discussion in Section IV showed that the fourth-order Runge–Kutta scheme is quite appropriate for time discretization in conjunction with the proposed wavelet-based spatial dis-

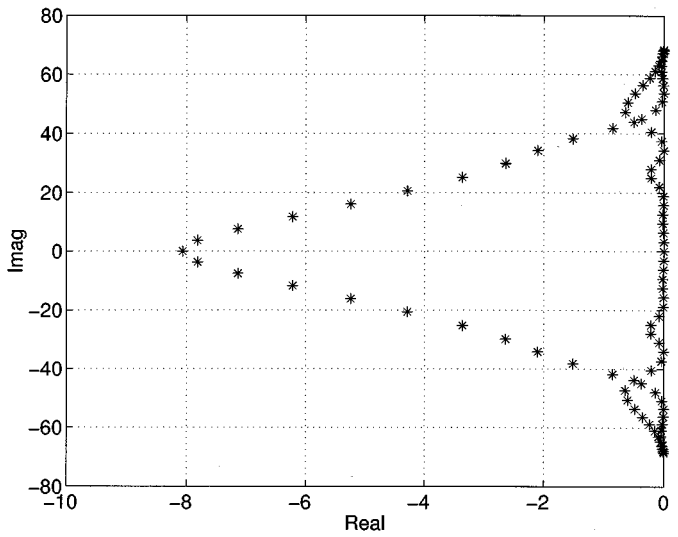

Fig. 10. Eigenvalues of the semidiscrete system arising from a normalized scalar line with $N = 50$ nodes. All eigenvalues have negative real part.

cretization (see also the discussion in [17]). Here, we briefly discuss the stability issues deriving from the termination of the scheme with some boundary conditions. These details were not reported in the main text not to interrupt the flow of the presentation.

We note that the equivalence between wavelet-based discretization and fourth-order finite differences holds only for internal coefficients. It can be proved that the modifications of the scaling functions and wavelets and the edges of the domain due to the interaction with the borders [15] lead to a terminated scheme with reduced order at the edges. Therefore, the terminated scheme is equivalent to high-order differences at internal nodes (leading to small dispersion errors during the propagation along the line) and to low-order differences at the edges. If we consider the terminated scheme and perform a stability analysis by looking at the eigenvalues of the semidiscrete system (8) in the case of linear terminations, we get only eigenvalues with nonpositive real part. This means that the spatial wavelet discretization with terminations is stable. The set of eigenvalues in the worst case of reflection coefficients $|\Gamma_{0,1}| = 1$ (either short-circuit or open-circuit terminations) is depicted in Fig. 10. It should be noted that the location of these eigenvalues in the complex plane is optimally suited to time discretization schemes like fourth-order Runge–Kutta, which is characterized by a stability region with approximately the same shape. We remark that high-order border differences often lead to late-time instabilities due to the presence of some eigenvalues with positive real part (see, e.g., [24]). Consequently, the order reduction at the edges must be regarded as an advantage since it insures late time stability of the discretized system. These considerations are well known in the literature. Further details can be found in [24] and references therein.

ACKNOWLEDGMENT

The author would like to thank Prof. Canavero for his constructive comments an Profs. Tabacco and Canuto for their significant help in understanding wavelets theory and developing wavelet bases on bounded domains. The author is also grateful to the anonymous reviewers for their constructive comments.

REFERENCES

[1] N. Balabanian and T. A. Bickart, *Electrical Network Theory*. New York: J. Wiley, 1969.
[2] C. E. Baum, J. B. Nitsch, and R. J. Sturm, "Analytical solution for uniform and nonuniform multiconductor transmission lines with sources," in *The Review of Radio Science, 1993–1996*. New York: URSI-Oxford Univ. Press, 1996.
[3] P. Besnier and P. Degauque, "Electromagnetic topology: Investigations of nonuniform transmission line networks," *IEEE Trans. Electromagn. Compat.*, vol. 37, pp. 227–233, May 1995.
[4] C. R. Burrows, "The exponential transmission line," *Bell System Tech. J.*, vol. 17, pp. 555–573, 1938.
[5] F. Chang, "Transient simulation of nonuniform coupled lossy transmission lines characterized with frequency-dependent parameters—Part I: Waveform relaxation analysis," *IEEE Trans. Circuits Syst. I*, vol. 39, pp. 585–603, Aug. 1992.
[6] A. Cohen, I. Daubechies, and J. Feauveau, "Biorthogonal bases of compactly supported wavelets," *Comm. Pure Appl. Math.*, vol. 45, pp. 485–560, 1992.
[7] W. Dahmen and C. Micchelli, "Using the refinement equation for evaluating integrals of wavelets," *SIAM J. Num. Anal.*, vol. 30, pp. 507–537, 1993.
[8] I. Daubechies, *Ten Lectures on Wavelets*. Philadelphia, PA: SIAM, 1992.
[9] R. A. DeVore, B. Jawerth, and V. A. Popov, "Compression of wavelet decompositions," *Amer. J. Math.*, vol. 114, pp. 737–785, 1992.
[10] T. Dhaene, L. Martens, and D. De Zutter, "Transient simulation of arbitrary nonuniform interconnection structures characterized by scattering parameters," *IEEE Trans. Circuits Syst. I*, vol. 39, pp. 928–937, Nov. 1992.
[11] S. Grivet-Talocia and F. Canavero, "Wavelet-based adaptive simulation of nonuniform interconnects with arbitrary loads," in *Proc. IEEE Int. Symp. Electromagn. Compat.*, Seattle, WA, Aug. 1999, pp. 450–455.
[12] ——, "Accuracy of propagation modeling on transmission lines," in *Proc. IEEE Int. Symp. Electromagn. Compat.*, Seattle, WA, Aug. 1999, pp. 474–479.
[13] ——, "Weak solution of the nonuniform multiconductor transmission lines," in *Proc. IEEE Int. Symp. Electromagn. Compat.*, Denver, CO, Aug. 1998, pp. 964–968.
[14] ——, "Wavelet-based adaptive solution for the nonuniform multiconductor transmission lines," *IEEE Microwave Guided Wave Lett.*, vol. 8, pp. 287–289, Aug. 1998.
[15] S. Grivet-Talocia and A. Tabacco, "Wavelets on the interval with optimal localization," *Math. Methods Models Appl. Sci.*, vol. 10, pp. 441–462, 2000.
[16] S. Grivet-Talocia and F. Canavero, "Weak boundary treatment for high order transient analysis of MTL's," in *Proc. IEEE Int. Symp. Electromagn. Compat.*, Washington, DC, Aug. 2000.
[17] B. Gustafsson, H. O. Kreiss, and J. Oliger, *Time Dependent Problems and Difference Methods*. New York: Wiley, 1995.
[18] "Special issue on wavelets in electromagnetics," *Int. J. Num. Modeling*, vol. 11, pp. 1–96, 1998.
[19] M. Krumpholz and L. P. B. Katehi, "MRTD: New time-domain schemes based on multiresolution analysis," *IEEE Trans. Microwave Theory Tech.*, vol. 44, pp. 555–571, Apr. 1996.
[20] M. Krumpholz, H. G. Winful, and L. P. B. Katehi, "Nonlinear time-domain modeling by multiresolution time domain (MRTD)," *IEEE Trans. Microwave Theory Tech.*, vol. 45, pp. 385–393, Mar. 1997.
[21] O. A. Palusinski, "Analysis of transients in nonuniform and uniform multiconductor transmission lines," *IEEE Trans. Microwave Theory Tech.*, vol. 37, pp. 127–138, Jan. 1989.
[22] C. R. Paul, *Analysis of Multiconductor Transmission Lines*. New York: Wiley, 1994.
[23] R. Robertson, E. Tentzeris, M. Krumpholz, and L. P. B. Katehi, "Modeling of dielectric cavity structures using multiresolution time-domain analysis," *Int. J. Num. Modeling*, vol. 11, pp. 55–68, 1998.
[24] B. Strand, "Numerical studies of hyperbolic IBVP with high-order difference operators satisfying a summation by parts rule," *Appl. Numer. Math.*, vol. 26, pp. 497–521, 1998.

[25] E. Tentzeris, R. Robertson, J. F. Harvey, and L. P. B. Katehi, "Stability and dispersion analysis of Battle–Lemarie based MRTD schemes," *IEEE Trans. Microwave Theory Tech.*, vol. 47, pp. 1004–1013, July 1999.
[26] V. K. Tripathi and N. Orhanovic, "Time-domain characterization and analysis of dispersive dissipative interconnects," *IEEE Trans. Circuits Syst. I*, vol. 39, pp. 938–945, Nov. 1992.
[27] J. R. Wait, *Electromagnetic Wave Theory*. New York: Harper Row, 1985.
[28] ——, *Electromagnetic Waves in Stratified Media*. New York: Pergamon Press, 1962.

Stefano Grivet-Talocia received the Laurea (*summa cum laude*) and Ph.D. degrees in electronic engineering from the Politechnic of Turin, Italy, in 1996 and 1998, respectively.

From 1994 to 1996, he was with NASA/Goddard Space Flight Center, Greenbelt, MD, where he worked on applications of fractal geometry and wavelet transform to the analysis and processing of geophysical time series. In 1996, he joined the Electromagnetic Compatibility Group, Electronics Department, Politechnic of Turin, working as a Researcher and Assistant Professor. His current research interests are in numerical modeling of TL structures and applications of wavelets to computational electromagnetics.

Dr. Grivet-Talocia has been serving as an Associate Editor for the IEEE TRANSACTIONS ON ELECTROMAGNETIC COMPATIBILITY since 1999.